ISSN: 2971-7760 | VOL 6, ISS 3 | 03 AUGUST 2026
https://doi.org/10.5281/zenodo.21778536
NASARAWA STATE UNIVERSITY, KEFFI, NIGERIA

SWARM INTELLIGENCE BASED PID TUNING FOR LOAD FREQUENCY CONTROL OF A TWO AREA POWER SYSTEM NETWORK

Nwaobasi Chukwuemeka Chijioke
gmexiss@gmail.com

ABSTRACT

This paper entails designing a Peripheral Integral Differential (PID) controller for a two area power system network using particle swarm optimization (PSO) technique which is a swarm based intelligence method. The load frequency for power system networks usually experience drop or fluctuations whenever there is a sudden engagement or disengagement of load. This is known as load disturbance. This research work aims to solve this problem by employing a PID controller to assist the governor control of the power system network. The effect of application of the PID controller is a stable load frequency operation even if there is a disturbance in the load. Also, the PID controller is usually tuned manually using the Zeigler-Nichols method. In the research work, however, the controller will be tuned with the help of the PSO algorithm. At the end of this research work, it will be shown that the two area power system network will maintain a steady load frequency even in the presence of disturbance. The LFC result will also be compared that of the manual tuning (referred to as base case) and that of the PSO tuning. The result will reveal that both methods are capable of stabilizing the load frequency but that the PSO tuned PID (PSO-PID) will give a superior result in terms of faster settling time.

KEYWORDS: Load frequency control, PID, PSO, Governor, Steam turbine, Power system, MATLAB.

INTRODUCTION

The increase in size and interconnectivity of electrical power systems has necessitated the evolution of load frequency control in order to stabilize and ensure reliability in power systems. Previously, this frequency control was essentially performed by manual adjustments and governor-based systems for maintenance of balance between generation and demand. However, with grid expansion, these systems were increasingly characterized with inadequacy. This set the blueprint for proportional-

ISSN: 2971-7760 | VOL 6, ISS 3 | 03 AUGUST 2026
https://doi.org/10.5281/zenodo.21778536
NASARAWA STATE UNIVERSITY, KEFFI, NIGERIA

integral control method which was hinged on automatic generation control. This automatic control enabled operators to automatically change generator outputs with respect to discrepancies in system frequency and tie-line power exchanges between interconnected areas; thus, establishing a significant shift from local control to coordinated, system-wide control. However, with increasing system dynamics and attendant uncertainties, these systems consistently displayed failure to handle system realities (Yousef et al., 2019). Furthermore, the restructuring of the global electrical power sector for over 30 years now, marked by deregulation and the integration of renewable energy sources, and the advancement of computational intelligence have further challenged the effectiveness of the conventional load frequency control mechanisms. Ahmad et al. (2020) stated that the unstable nature of renewable energy sources and the attendant reduction in system’s inertia which increases frequency fluctuations, are factors that challenge the effectiveness of these load frequency controllers. On the other hand, advancement in computational intelligence has given rise to load frequency control algorithms with intelligence that has been integrated into wide-area measurement systems as well as phasor measurement units. This paradigm has led to the emergence of techniques such as predictive control, robust control, and adaptive control, as highlighted in Guha et al. (2023); thus, the load frequency controller mechanism remains a critical component for grid stability and has continued to evolve in direct response to evolving complexity and uncertainties associated with power systems. To buttress this position, Sahu et al. (2022) had observed that metaheuristic algorithms like particle swarm optimization have tremendously improved system performance given different scenarios on deployment to optimize controller parameters, while Shayeghi et al. (2021) have reported even much more superlative performance in frequency stability when the PSO algorithm is combined with a predictive model.

Fathy and Kassem (2025) stated that such system constraints include generator ramp rates, tie-line limits, and operational reserves. What the MPC actually does is to dynamically adjust generation by anticipating load fluctuations, renewable variability, and disturbances. Akbar et al. (2022) stated that this quality is what makes the MPCs highly effective for frequency stabilization in interconnected grids. This is supported by Elsisi et al. (2024) who stated that MPCs performs superlatively in reducing nominal frequency deviations and tie-line oscillations when compared to the conventional approaches. However, the challenge with the MPC is the Nigeria scenario that lacks automation but this can be overcome with embedded controllers. As the world continues to adopt smart grid technologies, especially when variable renewables get integrated into the mix, MPC reliance will continue unchallenged. In essence, what happens

behind the scene is that PSO dynamically tunes prediction horizons, weighting factors, and control gains to ensure optimal system performance despite changing operating conditions; thus, this combination fully addresses
what had been criticized as MPC's reliance on accurate models, thereby forestalling the risk of suboptimal performance due to parameter mismatches. In fact, according to Jagatheesan et al. (2024), MPC provides a framework for predictive, constraint-based control, while PSO offers real-time tuning of MPC parameters, enhancing robustness under uncertainty.

MATERIALS AND METHODS

The methods and materials required for developing the model and model parameters of a two area hydro-thermal plant. In this work, the thermal area of the hydro-thermal plant will consist of two units of a thermal plant while the hydro area of the hydro-thermal plant will consist of two unit of a hydro plant. Two units each of a 500 MW thermal plant will be modelled while two unit of a 500MW hydro plant will be modelled. The turbines, the governors of these plants that serve as a primary control will be modelled. Also, the generators attached to the turbines of the thermal and hydro plants will be modelled.
In this work, it is intended that when there is a sudden change in the load on the generators attached to any of the plants, a secondary controller would be able to assist the primary controller (governor) to control a valve that will inject more steam (in the case of the thermal plant) or control the door of a penstock to release more flow of water (in the case of a hydro plant) so that more power would be applied to the shaft of the turbines and the frequency (load frequency) of the generator would remain constant and system stability would be maintained.
Without the secondary controller, the governor of both turbines might still be able to achieve stability. When the governor achieves stability, it might not be able to get the load frequency to its initial value before the disturbance was applied (Nikhil et al., 2016). As the disturbance increases for a system without a secondary controller, the load frequency continues to drop too until a point of complete instability will be reached (Lokkas et al., 2022). The secondary controller in this research work is a PID controller. Parameters of the PID controller will be tuned using the Particle Swarm Optimization (PSO) technique.

Materials

Modelling a thermal plant entails obtaining a Heat Balance Diagram (HBD) for the rated capacity of that plant. This research work aims to model a 500

ISSN: 2971-7760 | VOL 6, ISS 3 | 03 AUGUST 2026
https://doi.org/10.5281/zenodo.21778536
NASARAWA STATE UNIVERSITY, KEFFI, NIGERIA

MW capacity thermal plant. Therefore the HBD for a 500 MW thermal plant is obtained from Nikhil et al. (2016) and presented in figure 1.

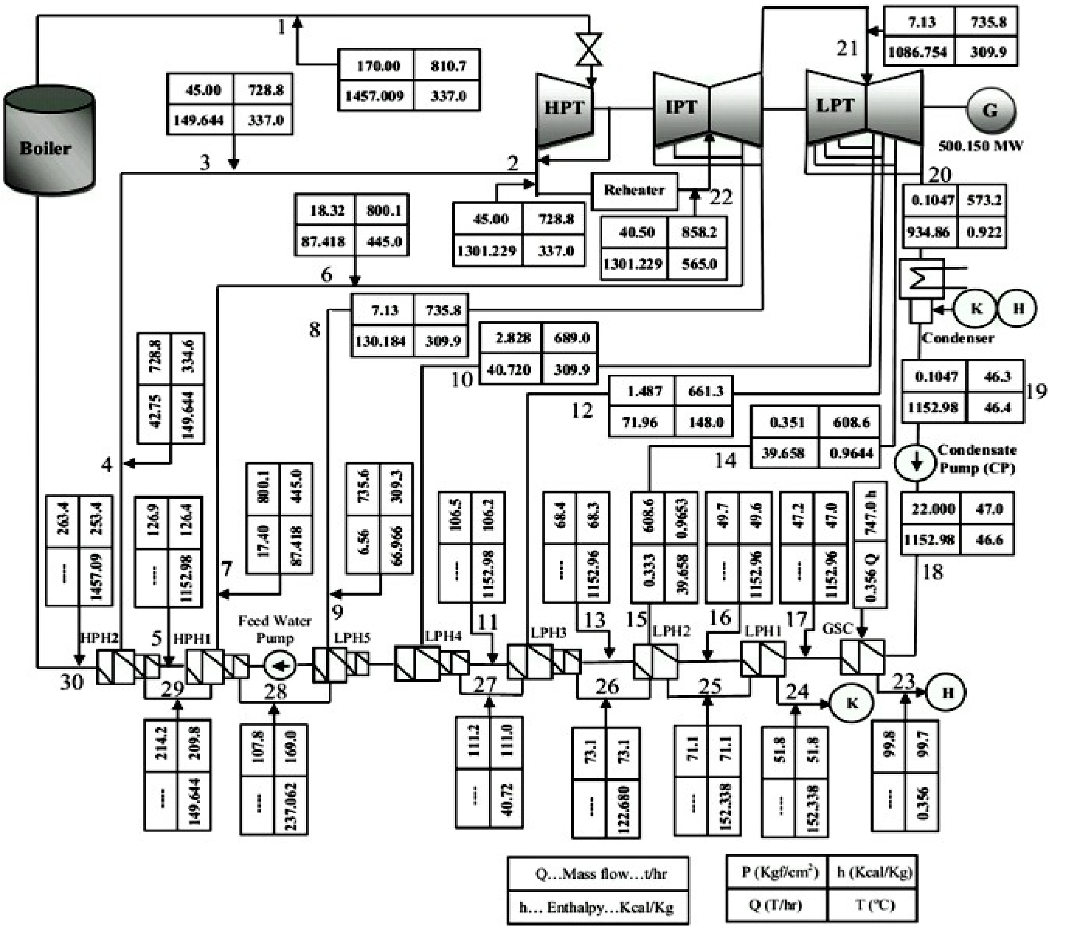

Figure 1 Heat balance diagram for a 500 MW thermal plant (Basu,

ISSN: 2971-7760 | VOL 6, ISS 3 | 03 AUGUST 2026
https://doi.org/10.5281/zenodo.21778536
NASARAWA STATE UNIVERSITY, KEFFI, NIGERIA

The heat balance diagram presents four thermal quantities that are useful in determining model parameter when designing the transfer functions for the plant model. These quantities are the mass flow of steam in tones per hour, the Enthalpy in kilocalories per kilogram (Kcal/Kg), the pressure of steam in kilogram force per centimeter squared (Kgf/cm^2) and temperature in degrees centigrade (^{0}C). The numbers shown in the diagram represents different stages in the flow or working of the thermal plant.

It is also important to state that the thermal plant that is modelled in this research work is one that is equipped with a Reheat Tandem Compound Steam turbine. This explains the HPT (High Pressure Turbine), IPT (Intermediate Pressure Turbine) and LPT (Low Pressure Turbine). These three structures make up the reheat configuration.

Another structure seen in figure 1 is the Boiler. This is where water is heated to high temperature and pressure before flowing, through valves and steam chest, to the HPT, IPT and LPT and then to the shaft of the generator.

Modelling of both plants will be done using the Simulink software in MATLAB. Therefore the MATLAB, release 2016 software, installed on a laptop running at 3.6 GHz processing speed and 12 GB of RAM memory will be employed.

3.2 Methods

The methods that will be applied in actualizing the aim and obectives of this work is presented

3.2.1 Mathematical model derivation (Transfer functions)

This section presents the derivation of transfer functions for both the thermal and hydro plants as separate entities, i.e. before hybridization.

3.2.1.1 Thermal plant transfer functions and Simulink model

The HBD diagram presented in figure 1 has three important sections that comprises of the Steam Chest (see the arrow designated 1 in the HBD of figure 1), the Reheat and the Cross Over (see the arrow designated 22 and 21 respectively in the HBD of figure 1). The steam chest will be designated SC, the reheat will be designated RH and the cross over will be designated CO.

Figure 2 presents the diagram showing the configurations of the steam turbine employed in this research work.

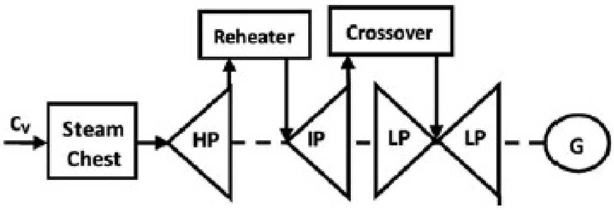

Figure 2 Steam turbine configuration (Nikhil et al.,

The configuration show the three main components of the thermal plant. Superheated steam moves from the boiler, through control valves (C_V see figure 2), to the steam chest from which it moves to the reheat section through the HPT to the cross over section through the IPT and then to the LPT from which it spins the turbine shaft that the generator (G, see figure 2) is connected to.

Figure 3 presents the dynamic model of the turbine.

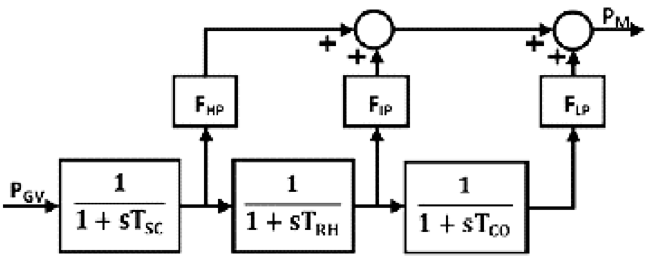

Figure 3 Steam turbine configuration (Nikhil et al.,

ISSN: 2971-7760 | VOL 6, ISS 3 | 03 AUGUST 2026
https://doi.org/10.5281/zenodo.21778536
NASARAWA STATE UNIVERSITY, KEFFI, NIGERIA

Figure 3 models a reheat tandem compound steam turbine where all three main components are captured in the model. These components are the SC, the RH and the CO.

The transfer function for the steam chest from figure 3:

$$tf_{SC}=\frac{1}{1+sT_{SC}} \qquad (1)$$

Where tf_{SC} is the transfer function of the steam chest and
T_{SC} is the time constant of the steam chest

T_{SC} represents the time it takes the valve (see valve directly above HPT in figure 1) to respond to the control system (governor and PID) attached to the plant.

The transfer function for the Reheat turbine, from figure 3 is given as:

$$tf_{RH}=\frac{1}{1+sT_{RH}} \qquad (2)$$

Where tf_{RH} is the transfer function of the reheat turbine and
T_{RH} is the time constant of the reheat turbine.

The transfer function for the Cross over, from figure 3 is given as:

$$tf_{CO}=\frac{1}{1+sT_{CO}} \qquad (3)$$

Where tf_{CO} is the transfer function of the Cross over and
T_{CO} is the time constant of the cross over

Three other blocks are seen from figure 3. These blocks are the power fraction blocks. The power fraction is the proportion of the total power transferred from each of the three main stages of the reheat tandem compound steam turbine. Therefore:

F_{HP} represents the power fraction of the high pressure turbine
F_{IP} represents the power fraction of the intermediate pressure turbine and
F_{LP} represents the power fraction of the low pressure turbine

The power fractions from all three stages are combined using circular shaped combination block. Also, form figure 3:

P_M is the mechanical power output of the system while the input
P_{GV} is the power supplied by the governor of the system
By applying block diagram reduction technique on figure 3, the equivalent transfer function (ration of P_M and P_{GV}) for the reheat tandem compound steam turbine, $T_{REHEAT}(S)$ is calculated thus:

$$T_{REHEAT}(S)=\left\{\left(F_{IP}+\frac{F_{LP}}{(1+sT_{CO})}\right)\frac{1}{(1+sT_{RH})}+F_{HP}\right\}\frac{1}{(1+sT_{SC})} \tag{4}$$

$$T_{REHEAT}(S)=\left\{\frac{F_{IP}}{(1+sT_{RH})}+\frac{F_{LP}}{(1+sT_{CO})(1+sT_{RH})}+F_{HP}\right\}\frac{1}{(1+sT_{SC})} \tag{5}$$

$$T_{REHEAT}(S)=\frac{F_{IP}}{(1+sT_{RH})(1+sT_{SC})}+\frac{F_{LP}}{(1+sT_{CO})(1+sT_{RH})(1+sT_{SC})}+\frac{F_{HP}}{(1+sT_{SC})} \tag{6}$$

$$T_{REHEAT}(S)=\frac{F_{IP}(1+sT_{CO})+F_{LP}+F_{HP}(1+sT_{CO})(1+sT_{RH})}{(1+sT_{CO})(1+sT_{RH})(1+sT_{SC})} \tag{7}$$

Expanding numerator and denominator of equation (7):

$$T_{REHEAT}(S)=\frac{(F_{HP}+F_{IP}+F_{LP})+(F_{HP}T_{CO}+F_{IP}T_{CO}+F_{HP}T_{RH})s+(F_{HP}T_{CO}T_{RH})s^2}{1+(T_{CO}+T_{RH}+T_{SC})s+(T_{CO}T_{RH}+T_{CO}T_{SC}+T_{RH}T_{SC})s^2+(T_{CO}T_{RH}T_{SC})s^3} \tag{8}$$

F_{HP}, F_{IP}, and F_{LP} are expressed in per unit. This means that:

$$F_{HP}+F_{IP}+F_{LP}=1 \tag{9}$$

ISSN: 2971-7760 | VOL 6, ISS 3 | 03 AUGUST 2026
https://doi.org/10.5281/zenodo.21778536
NASARAWA STATE UNIVERSITY, KEFFI, NIGERIA

Therefore equation (8) becomes

$$T_{REHEAT}(S)=\frac{1+(F_{HP}T_{CO}+F_{IP}T_{CO}+F_{HP}T_{RH})s+(F_{HP}T_{CO}T_{RH})s^2}{1+(T_{CO}+T_{RH}+T_{SC})s+(T_{CO}T_{RH}+T_{CO}T_{SC}+T_{RH}T_{SC})s^2+(T_{CO}T_{RH}T_{SC})s^3} \tag{10}$$

Or rearranging to suit the Simulink software:

$$T_{REHEAT}(S)=\frac{(F_{HP}T_{CO}T_{RH})s^2+(F_{HP}T_{CO}+F_{IP}T_{CO}+F_{HP}T_{RH})s+1}{(T_{CO}T_{RH}T_{SC})s^3+(T_{CO}T_{RH}+T_{CO}T_{SC}+T_{RH}T_{SC})s^2+(T_{CO}+T_{RH}+T_{SC})s+1} \tag{11}$$

Equation (10) or equation (11) gives the transfer function for the reheat tandem compound steam turbine.
The transfer function (tf_G) for the governor (mechanical governor) of the thermal plant according to (Wang et al., 2020) is given as:

$$tf_G=\frac{1}{(1+sT_G)} \tag{12}$$

Where T_G is the time constant of the governor. This reveals the response time of the turbine power (P_M) output changes to a change in valve opening for control of steam into the turbine.

For stable operation of the governor of a turbine, they are designed with a droop characteristic. This helps the governor to increase the speed of the generator whenever there is an increase in the load without overcorrecting and leading wild oscillations (runaway) characterized by instability.
The droop is defined mathematically as

$$R(\%)=\frac{frequency\ change(\%)}{power\ output\ change(\%)}x\,100 \tag{13}$$

This research work entails modelling hybridization of a hydro and thermal system. The thermal system, in this work, will be composed of two units of a thermal plant and a single unit of a hydro plant. This means that multiple droops will be connected. Therefore the equivalent droop (R_{eq}) for their governors will be:

$$R_{eq}=\frac{1}{\frac{1}{R_1}+\frac{1}{R_2}+\frac{1}{R_3}} \tag{14}$$

Where R_1, R_2 and R_3 are individual droops for the governors for each of the thermal plant and that of the hydro plant.

For the generator model, according to Atkinson and Albayati (2021), the changes in mechanical power ΔP_m and electrical power ΔP_e of a generator can be expressed as:

$$\Delta P_m+\Delta P_e=2H_{eq}\frac{d}{dt}(\Delta w_m) \tag{15}$$

Where Δw_m (rad/s) is the change in the angular velocity of the shaft, H_{eq} is the equivalent angular inertia constant of the generator.
The change of electrical power ΔP_e due to changes in frequency can be expressed as:

$$\Delta P_e=\Delta P_L-D.\Delta w_m \tag{16}$$

Where:
ΔP_L is a non-frequency sensitive load change, D.
Δw_m is a frequency sensitive load change, and
D is the load damping constant.

The damping constant captures the effect of frequency-sensitive load. The load damping constant symbolizes the lumped percent change in the load for a 1% change in frequency.

Substituting the value of ΔP_e in equation (16) into equation (15):

$$\Delta P_m+\Delta P_L=2H_{eq}\frac{d}{dt}(\Delta w_m)+D.\Delta w_m \tag{17}$$

Applying Laplace transform to equation 17 gives:

$$\Delta P_m+\Delta P_L=\Delta w_m(2H_{eq}s+D)$$

ISSN: 2971-7760 | VOL 6, ISS 3 | 03 AUGUST 2026
https://doi.org/10.5281/zenodo.21778536
NASARAWA STATE UNIVERSITY, KEFFI, NIGERIA

Therefore:

$$\frac{\Delta w_m}{\Delta P_m + \Delta P_L} = \frac{output}{input} = \frac{1}{(2H_{eq}s + D)} \quad (18)$$

Equation (18) can be written in the form of a standard first-order transfer function as:

$$\frac{\Delta w_m}{\Delta P_m + \Delta P_L} = \frac{output}{input} = \frac{K_P}{(T_P s + 1)} \quad (19)$$

Where $K_P = \frac{1}{D} = power\ system\ gain$ (20)

¿ $T_P = \frac{2H_{eq}}{D} = power\ system\ time\ constant$ (21)

Now H_{eq} which is the equivalent angular inertia constant of the combined generator in a particular area.

H_{eq} is therefore calculated as:

$$H_{eq} = \frac{H_1 S_1 + H_2 S_2}{S_1 + S_2} \quad (22)$$

H_1 and H_2 represent inertia constant for generator one and generator two (since two units of thermal plant or generators will be combined in area 1) S_1 and S_2 represents the sum of the power of each of the individual generators (two).

3.2.1.3 Secondary controllers

The governor (primary controller) of a turbine in a plant is capable of controlling the load frequency and keeping the system stable even in the presence of disturbance. However this capability is limited in the sense that the governor might not be able to get the frequency change back to zero after responding to load disturbance resulting to reduced speed of the generator even though the system is stable.

This begs for the need for secondary controllers. In this research work, two secondary controller will be employed. A PID controller and an MPC controller. The PID parameter will be tuned using the Particle Swarm

Optimization Technique and, also, the PID will be combined with the MPC controller and tuned with the same PSO algorithm (MPC-PSO) with an aim to always get the change in frequency to zero whenever there is a load disturbance.

Figure 3.6 presents a Simulink model of a two unit thermal plant.

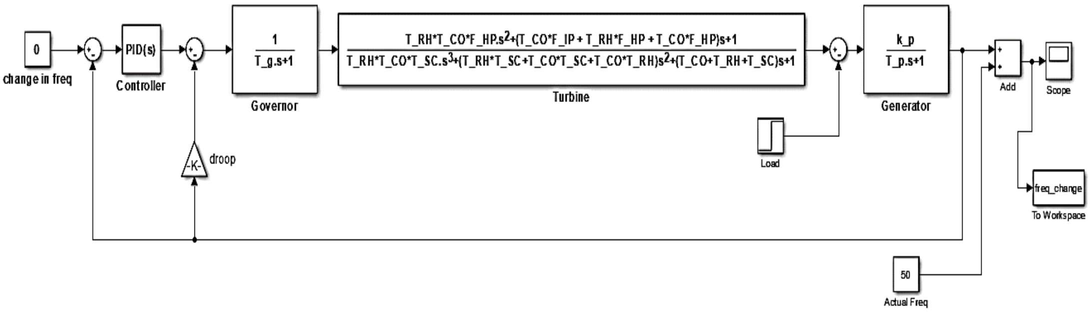

Figure 4 Thermal plant model (Two units) for

Figure 3.6 presents a Simulink model for a two unit thermal plant in area one. The two units design for the model is reflected in inertia constant of the generator presented in equation (22). The two units design is also reflected in the droop characteristic of the governor presented in equation (14). The time constant calculations for all components (turbine, generator and governor) of the model presented in figure (3.6) will be presented in subsequent sections and will also reflect the two unit design.

3.2.1.4 Hydro plant transfer function and Simulink model

The second area of the hydrothermal plant will consist of a single unit hydro plant. Figure 3.7 presents a simplified schematic diagram of a hydro power plant.

ISSN: 2971-7760 | VOL 6, ISS 3 | 03 AUGUST 2026
https://doi.org/10.5281/zenodo.21778536
NASARAWA STATE UNIVERSITY, KEFFI, NIGERIA

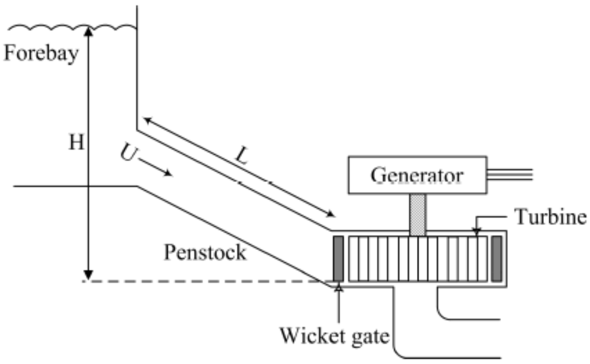

Figure 5 Hydro power

Where:
L is the length of the penstock,
U is the velocity of the water
H is the height of water (water head)

The turbine is majorly a hydraulic turbine-penstock and its simplified transfer function, according to Naghizadeh et al. (2022) is presented in equation (23)

$$tf = \frac{1 - s\,T_w}{1 + 0.5\,s\,T_w} \tag{23}$$

Where T_w is the water starting time, that represents the time required for a head H to accelerate the water in the pen stock from stand still to the velocity U. The time constant T_w is calculated as:

ISSN: 2971-7760 | VOL 6, ISS 3 | 03 AUGUST 2026
https://doi.org/10.5281/zenodo.21778536
NASARAWA STATE UNIVERSITY, KEFFI, NIGERIA

$$T_w = \frac{LU}{a_g H} = \frac{L \frac{Q_r}{\pi r^2}}{a_g H} \tag{24}$$

Where Q_r is the discharge rate of the penstock in m^3/s, and r is the radius of the penstock cross-section, a_g is acceleration due to gravity. T_w varies with operating point. Its value mainly depends on U, because other parameters remain almost unchanged.

The simplified transfer function tf_{gov} of the governor of the hydro power plant is presented in equation (3.25).

$$tf_{gov} = \frac{1}{1 + s T_h} \tag{25}$$

Where T_h is the time constant of the governor of a hydro power plant as distinct from equation (12). T_h is usually larger than T_G (equation (12)) due to the opening of the door of the penstock as a result of servo motor actions.

The generator used in area two (hydro power plant area) is assumed to be of the same type and characteristic as the one employed in area one. Therefore they possess the same transfer function.

Therefore the Simulink model of the single unit hydro power plant of area two is presented in figure 3.8.

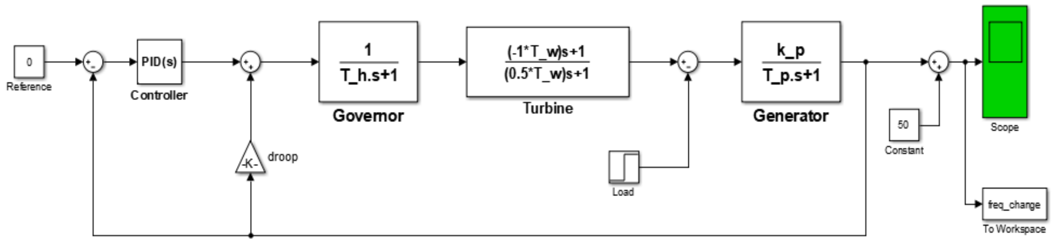

Figure 6 Hydro plant

Figure 7 therefore presents the final model for the hydro-thermal plant designed in this research work

ISSN: 2971-7760 | VOL 6, ISS 3 | 03 AUGUST 2026
https://doi.org/10.5281/zenodo.21778536
NASARAWA STATE UNIVERSITY, KEFFI, NIGERIA

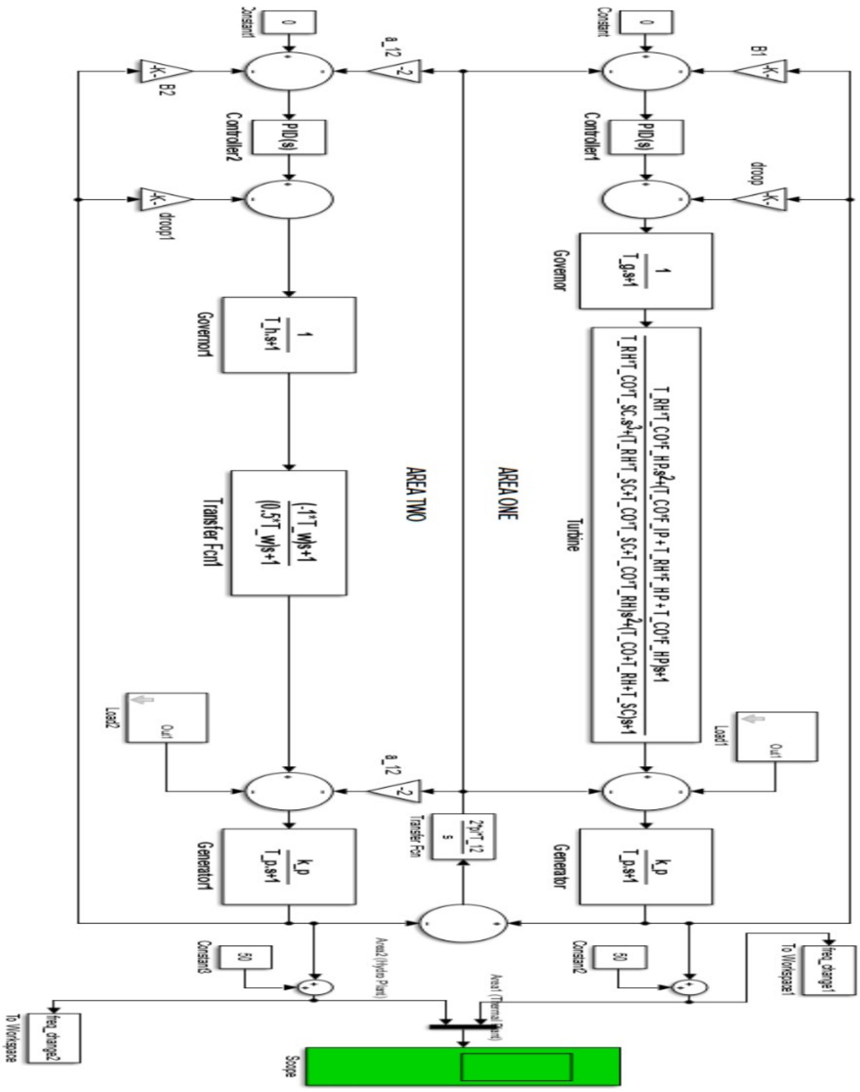

Figure 7 Hydro-thermal plant model for two areas

ISSN: 2971-7760 | VOL 6, ISS 3 | 03 AUGUST 2026
https://doi.org/10.5281/zenodo.21778536
NASARAWA STATE UNIVERSITY, KEFFI, NIGERIA

3.2.4 PSO Algorithm

In this research work, the PSO algorithm will be used to tune the secondary controller for both plants in hydro-thermal plant model. At the beginning of the particle swarm optimization algorithm, population of particles with random positions is initialized. Each member of the

population is called a particle. Each particle will have the P, I and D values of the PID controller as its coordinates or position. This is a three dimensional problem and so a three dimensional search space will be created for the particles.
The three dimensional search space is all possible combination of the P, I and D parameters. In this research work, a search space between 1 and 50 is chosen for each of the P, I and D parameters. The search space was arrived at after discovering, during manual tuning, that any parameter above 50 will result in very violent system response that will not be feasible in real life. Another consideration, though secondary, is the fact that the larger the search space, the more likely the particles get stuck in a local minima instead of a global minima. This can be solved by increasing the population of particles as the search space increases which takes a very huge toll on processing speed.
On executing the algorithm, the particle then begin to search (within the search space) for the optimum PID gains by updating their position using a position and a velocity equation. Equation (26) presents the velocity equation used in PSO algorithm.

$$v_{ijk}(t+1)=w(t)v_{ijk}(t)+c_1r_1(pbest_{ijk}(t)-x_{ijk}(t))+c_2r_2(gbest_{ijk}(t)-x_{ijk}(t)) \quad (26)$$

Where $v_{ij}(t+1)$ is the velocity of the particle after the ($t+1$)th iteration and $v_{ij}(t)$ is the velocity of the particle at the (t)th iteration. The parameter $w(t)$ denotes the weights employed (randomly selected at the beginning of the iteration) while the variables c and r are social variable that are also randomly initialized.
$x_{ijk}(t)$ is the position of the particles and the subscripts *ijk* signifies the particles position in the three dimensional space.

The velocity equation pushes the particle to a new position. The position is updated using equation (26)

$$x_{ij}(t+1)=x_{ij}(t)+v_{ij}(t+1) \quad (27)$$

Where $x_{ijk}(t+1)$ is the position of the particle after the ($t+1$)th iteration and $x_{ijk}(t)$ is the position of the particle at the (t)th iteration and $v_{ij}(t+1)$ is the position calculated in equation (26)

The algorithm then calculates the cost of moving each particle to a new position. The cost is calculated by running the simulation for each of the

particle (P, I and D values of that particle) and grabbing the frequency data. The frequency data is then fed to an objective function. The particle with the lowest cost becomes PBEST (particle best). PBEST might be a particle at a local minima or even a global minima. As the iteration continues, if a global minima is attained by a particle, that particle becomes GBEST (global best) and becomes the solution to the problem. Meaning the P, I and D parameters that represent the particle position becomes the tuned parameter for the PID controller.
It is also important to state that the moment a global minima is established by a particle, all other particles begin to drift towards that position after which convergence of the solution occurs.

3.2.4.1 Objective function formulation

The objective function helps the PSO algorithm to calculate the cost of moving a particle from one position to another after every epochs or iterations. This is done by feeding the P, I and D parameter of a particle at an epoch (or an iteration) to the model and running the simulation. Frequency data is then grabbed from the simulation and fed to certain statistical tool that helps in calculating the cost of moving the particle. This cost is essentially frequency errors that are seen as over shoots settling time and steady state errors. Therefore the particle with the least cost or least error is selected as the solution. That particle no longer have reason to move and it stays in that position while other particles navigates towards it.
In this research work the Integral of Time-weighted Absolute Error (ITAE) function will be selected as the objective function of the PSO algorithm. This is because this function takes care of errors like settling time, overshoots, and steady state error.
The ITAE is defined as:

$$ITAE = \int_{0}^{T} t\left|e(t)\right| dt \tag{28}$$

Where t is time, $|e(t)|$ is absolute error and T is the simulation time (time the simulation stops).

$|e(t)|$ is the absolute difference between the desired frequency and the frequency calculated. By multiplying time with the absolute error, the ITAE penalizes minor errors thereby taking care of overshoots, settling time and steady state error.

ISSN: 2971-7760 | VOL 6, ISS 3 | 03 AUGUST 2026
https://doi.org/10.5281/zenodo.21778536
NASARAWA STATE UNIVERSITY, KEFFI, NIGERIA

The above function (equation 28) is achieved in MATLAB by employing the *trapz()* function and providing time and error data as input arguments. This data is gotten by connecting a "*to workspace*" Simulink block in the designed model (see figure 7).

Since two areas are modelled, the ITAE is calculated for both areas and the cost returned to the PSO algorithm. Equation 29 illustrates this point

$$cost = ITAE_1 + ITAE_2 = \int_0^T t_1 |e_1(t)| dt + \int_0^T t_2 |e_2(t)| dt$$

The subscripts signifying area 1 and area 2

$$cost = \int_0^T \left[t_1 |e_1(t)| + t_2 |e_2(t)| \right] dt \qquad (29)$$

Therefore the particle with lowest cost becomes the solution or the tuned PID parameters.

3.2.5.1 PID design

Figure 8 presents the PID controller design

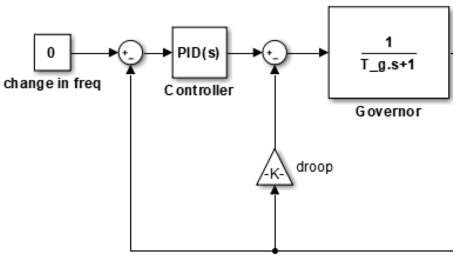

Feedback from output of

Figure 8 PID controller

The PID controller Simulink block is seen attached behind the governor of a particular power plant. This is to provide secondary assistance to the

ISSN: 2971-7760 | VOL 6, ISS 3 | 03 AUGUST 2026
https://doi.org/10.5281/zenodo.21778536
NASARAWA STATE UNIVERSITY, KEFFI, NIGERIA

governor. The controller is fed with the *change in freq* block. This is essentially a constant Simulink block that have a value of zero. A feedback from the generator output (frequency) is fed to the PID block. The PID then compares this value with the value provided in the constant block (which is zero) and adjust valves or doors of penstock to inject more steam or water in order to keep the frequency constant.

The PID achieves frequency control depending on the tuned P, I and D values.

The PID parameter will be tuned manually using the Zeigler-Nichols method. The manual tuning will be referred to as base line performance of the system.

3.2.5.2 Zeigler-Nichols tuning

In the Zeigler-Nichols tuning methods, apart from the P value, all other parameters are set to zero. The P value is then increased until sustained oscillations is observed. Figure 9 presents the sustained oscillations observed in both areas.

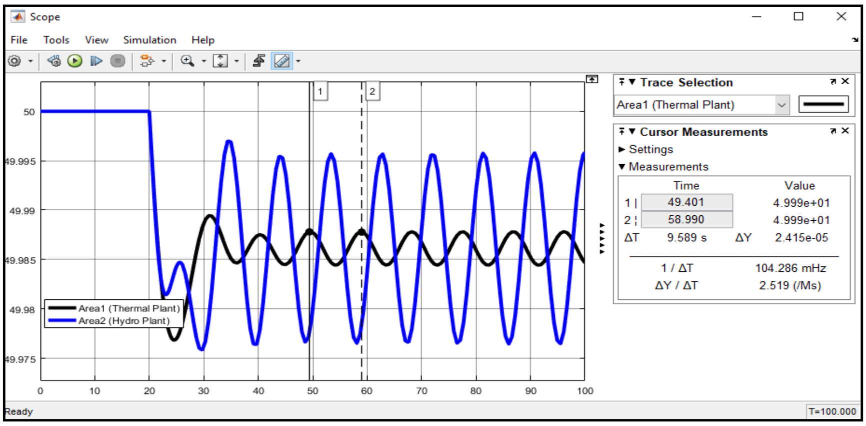

Figure 9 PID tuning area one

The value of P that produces the sustained oscillations is the critical gain and denoted as K_C. this value is seen to be:

$K_C = 27.8$

And the frequency for this sustained oscillation is:

$$f_0 = \frac{1}{\Delta T} = \frac{1}{9.589} = 0.1043\,Hz$$

ΔT is seen from the cursor measurement tool shown in figure 9

Then for area one (black wave form) and according to Zeigler-Nichols method:

$P = 0.6 \times K_C = 0.6 \times 27.8 = 16.68$

$I = 2.0 \times f_0 = 2 \times 0.1043 = 0.2086$

$D = 0.125 / f_0 = 0.125/0.1043 = 1.1985$

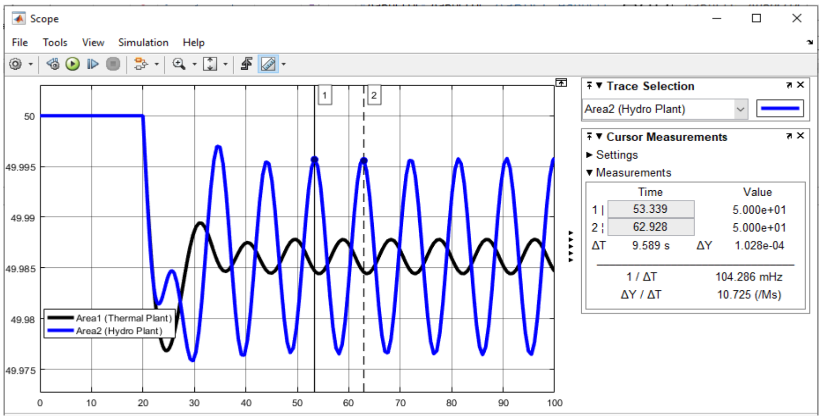

Figure 10 PID tuning area two

For area two (blue waveform) consider figure 10

Note that the same K_C value produce both waveforms. Observe also that ΔT = 9.589 s. This is the same value seen in figure 9. Therefore the PID

parameter for both areas are the same. This makes sense as PID parameters of both areas cannot be different since the system was synchronized using tie line during hybridization.
Therefore the base line PID parameter for both areas is:

P = 16.68, I = 0.2086 and D = 1.1985

Results

The results of this research is presented in such a form that not only portrays performance evaluation of the system.

In all scenarios, the simulation will run for 100 seconds and the load disturbance will be applied 20 seconds after the simulation has started.

System base line performance

Results for the system base line performance is presented in this section. The base line performance is the performance of the system when tuned manually. This is the performance of the system when P = 16.68, I = 0.2086 and D = 1.1985.

No load disturbance

Results for no load disturbance is presented in figure 11. For no load disturbance, the magnitude of the step function used to simulate load is set to zero.

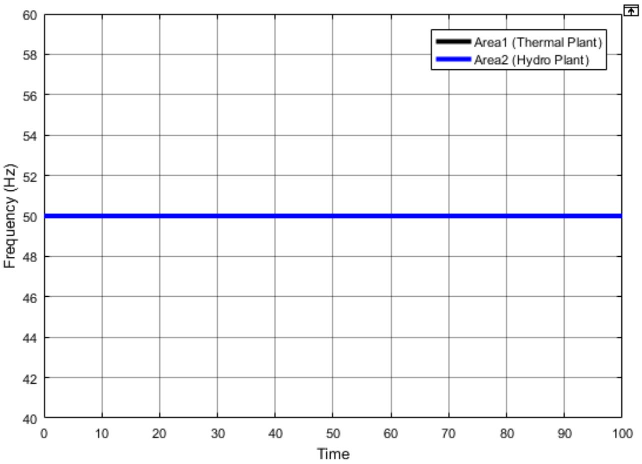

Figure 11 No load

ISSN: 2971-7760 | VOL 6, ISS 3 | 03 AUGUST 2026
https://doi.org/10.5281/zenodo.21778536
NASARAWA STATE UNIVERSITY, KEFFI, NIGERIA

One unit of power load disturbance at area one only

The result for one unit of power load disturbance at area one is presented in figure 12.

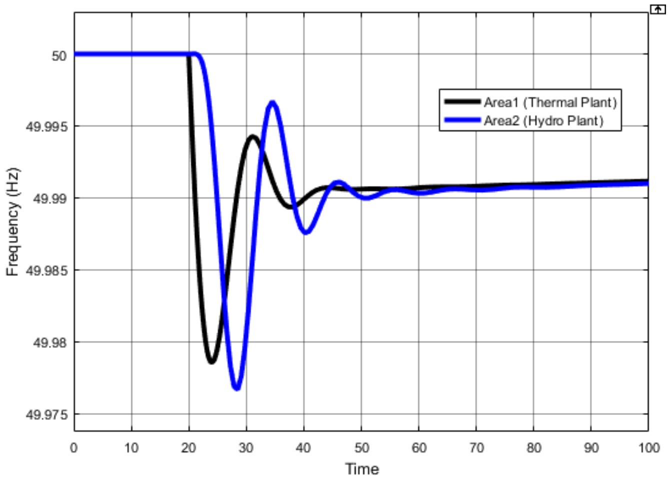

Figure 12 Load disturbance at area one

One unit of power load disturbance at area two only

ISSN: 2971-7760 | VOL 6, ISS 3 | 03 AUGUST 2026
https://doi.org/10.5281/zenodo.21778536
NASARAWA STATE UNIVERSITY, KEFFI, NIGERIA

The result for one unit of power load disturbance at area two is presented in figure 13

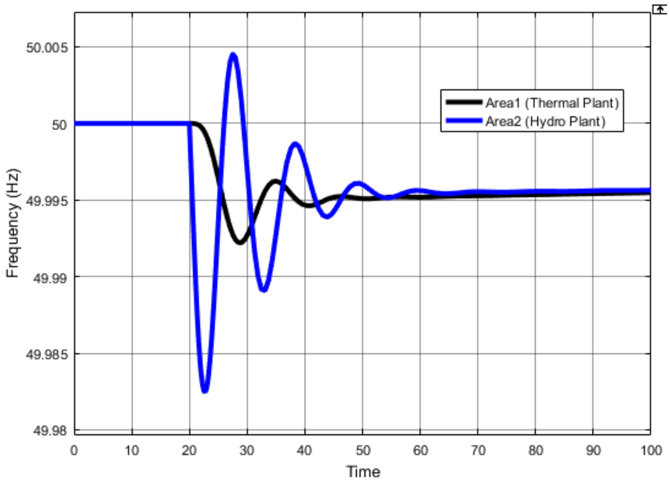

Figure 13 Load disturbance at area two

One unit of power load disturbance simultaneously at both areas

The result for one unit of power load disturbance at both areas simultaneously is presented in figure 14.

ISSN: 2971-7760 | VOL 6, ISS 3 | 03 AUGUST 2026
https://doi.org/10.5281/zenodo.21778536
NASARAWA STATE UNIVERSITY, KEFFI, NIGERIA

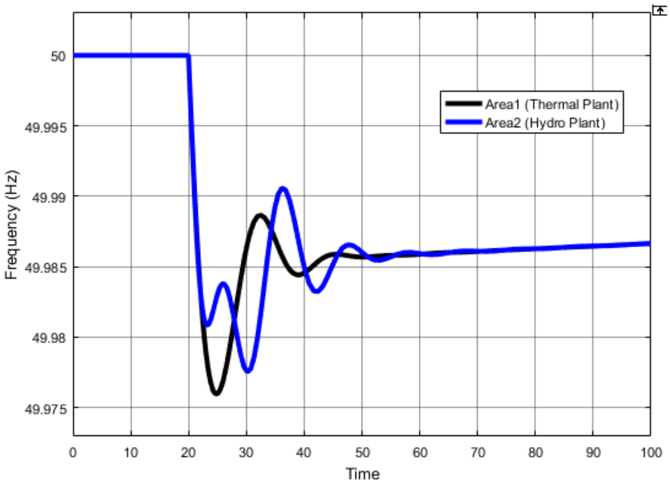

Figure 14 Load disturbance at both

System performance using tuned PID parameters from PSO

Before presenting the system performance under the tuned PID parameters, the PSO results will be presented

PSO result

The PSO result is presented in figure 15. Four results are presented. The top left being the particle search space, the top right being the particle convergence. The bottom left being the simulation convergence plot and the bottom right being the print out from the simulation revealing the P, I and D parameter result.

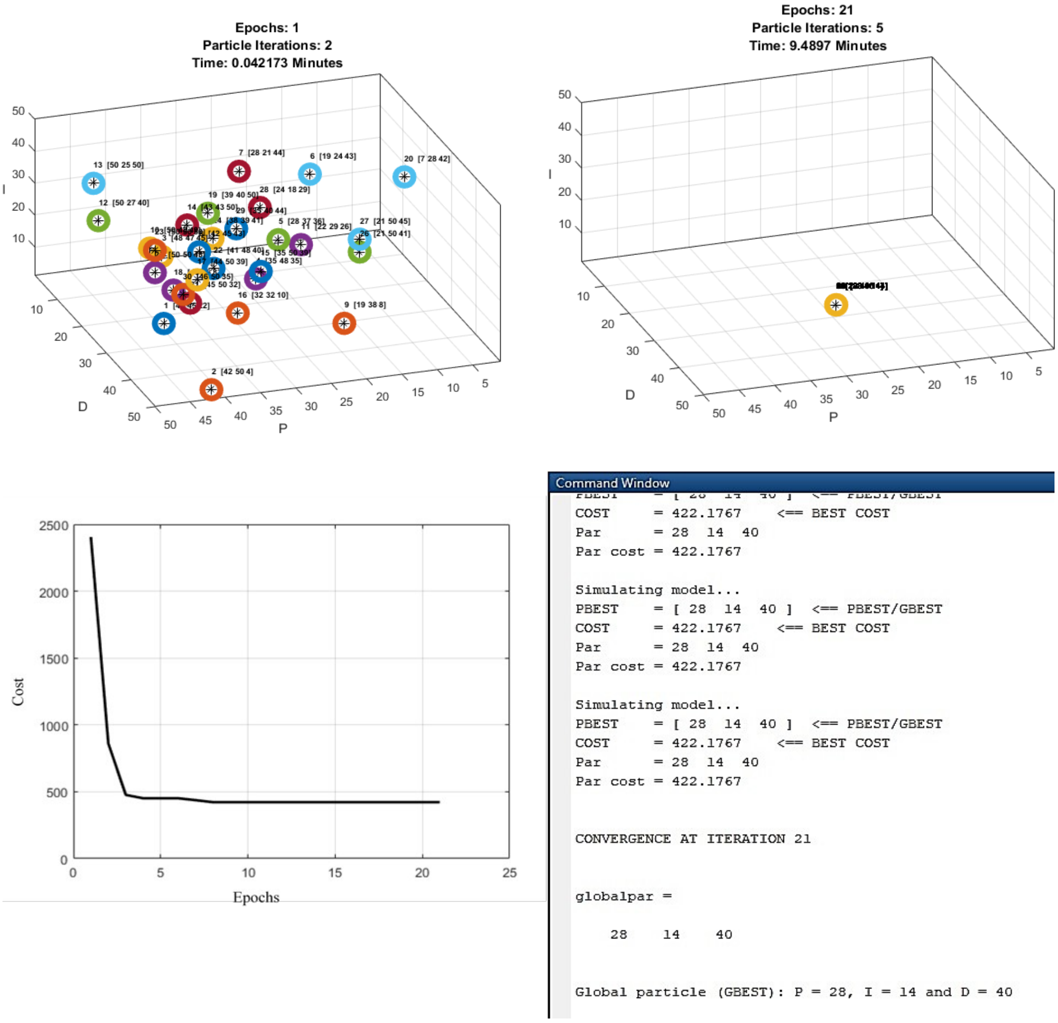

Figure 15 PSO result

ISSN: 2971-7760 | VOL 6, ISS 3 | 03 AUGUST 2026
https://doi.org/10.5281/zenodo.21778536
NASARAWA STATE UNIVERSITY, KEFFI, NIGERIA

From the result, P = 28, I=14 and D = 40

Performance with 1 unit of power disturbance at area one only

Results from the performance of the system after tuning with PSO and when only area one is subjected to one units of power disturbance is presented in figure 16

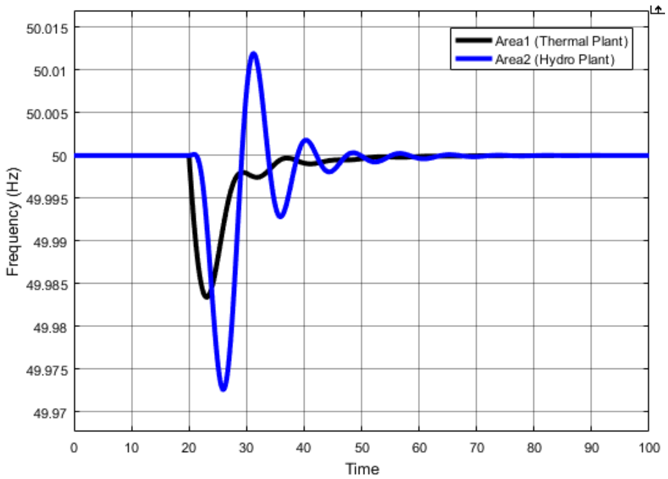

Figure 16 PSO result: load disturbance on

ISSN: 2971-7760 | VOL 6, ISS 3 | 03 AUGUST 2026
https://doi.org/10.5281/zenodo.21778536
NASARAWA STATE UNIVERSITY, KEFFI, NIGERIA

4.1.2.3 Performance with 1 unit of power disturbance at area two only

Results from the performance of the system after tuning with PSO and when only area two is subjected to one units of power disturbance is presented in figure 17

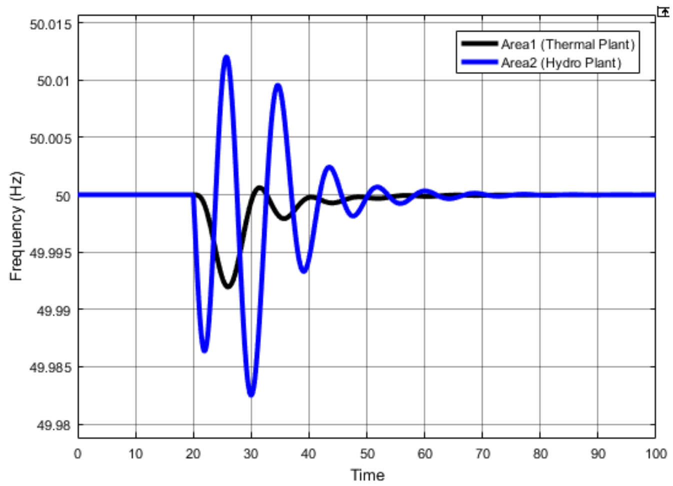

Figure 17 PSO result: load disturbance on

ISSN: 2971-7760 | VOL 6, ISS 3 | 03 AUGUST 2026
https://doi.org/10.5281/zenodo.21778536
NASARAWA STATE UNIVERSITY, KEFFI, NIGERIA

Frequency, Turbine speed and load comparism

Figure 18 presents result obtain from comparing frequency, turbine speed of the generators of both areas. Figure 18 also shows the load disturbance exerted on the systems in both areas.

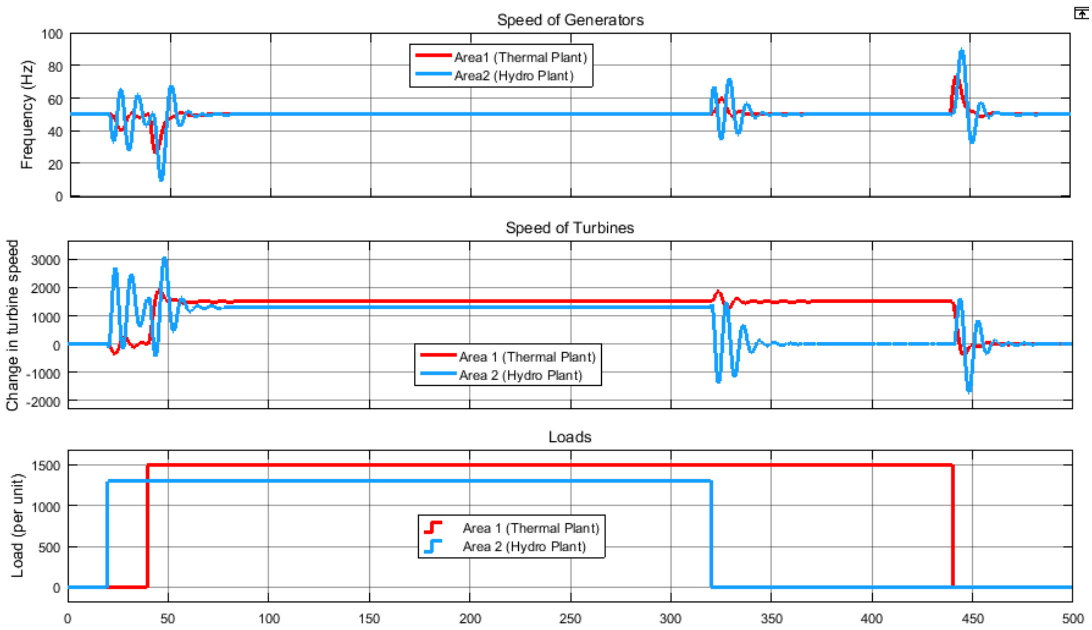

Figure 18 Frequency, Turbine speed and Load graph

Discussions

This section discusses the results obtained and presented in figure 11 through figure 4.18. It is important to state that a disturbance in a single area will trigger frequency response in both areas. This is because the model composes of a hybrid of two different power plant. The responses will again be diffferent.
Also the system is designed using the per unit system of measurement, therefore the disturbances will also be in the form of per unit. All disturbances applied are in a single unit of power and are applied 20 seconds into the simulation time.

Figure 11 presents the result obtained when there is no disturbance in any of the areas. The figure shows a flat line at 50 Hz. This means the system is correctly modelled as there is no need for the governor or any of the secondary controllers to make any adjustments in any of the areas so both areas show an overlapping flat line.

In figure 12 the system is running at its base line or base case and it presents the result obtained when there is a unit power of load disturbance applied at area one only. The result presented show two graphs (blue and black) that represents frequency responses from the two areas. The black graph represent the response of the thermal plant. This is normal as a disturbance in one area will trigger frequency response, that are different, in both areas. The blue graph represents the response of the system at area two (hydro plant). It is observed that this response is clearly slower than the response in area one. This is due to the time constant of the governor in the hydro area beign higher than that of the governor in area one. This increased time constant is due to longer servo motor actions required to open gates of penstock.

In figure 13 the system is still running at its base line or base case and it presents the result obtained when there is a unit power of load disturbance applied at area two only. The result presented show two graphs (blue and black) that represents frequency responses from the two areas. The black graph represent the response of the thermal plant. This is normal as a disturbance in one area will trigger frequency response, that are different,

ISSN: 2971-7760 | VOL 6, ISS 3 | 03 AUGUST 2026
https://doi.org/10.5281/zenodo.21778536
NASARAWA STATE UNIVERSITY, KEFFI, NIGERIA

in both areas. The blue graph represents the response of the system at area two (hydro plant). Again it is observed that this response is still slower than the response in area one.

In figure 14 the system, still running at its base line or base case, presents the result obtained when there is a unit power of load disturbance applied simultaneously at both areas. The result presented show two graphs (blue and black) that represents frequency responses from the two areas. The black graph represent the response of the thermal plant. This is normal as a disturbance in one area will trigger frequency response, that are different, in both areas. The blue graph represents the response of the system at area two (hydro plant). Again it is observed that this response is still slower than the response in area one.
This scenario is an ideal case because in real life it will be almost imposible to have disturbances applied at the same time and magnitude to the same area.

Results presented from figures 12 to figure 14 did not get the frequency back to 50 Hz. This is because the system is runing at its base case. Even thought the system maintained stability, the generator speed did not recover.

Figure 15 present the PSO results and are in four parts as seen in the figure. The top left figure shows the particle initialization in the three dimensional search space. The particle population is programmed to be 60 percent of the search space. The search space is 50 for each of the P, I and D solutions. Therefore 30 particles are initialized in the search space. This 60 percent value is just a programming choice and is chosen because after running the algorithm several times it is seen that at that value the particles are never stuck in a local minima.
The top right corner of figure shows the convergence of all particles in the search space. The coordinates of the converged particles represents the tuned P, I and D parameters. The bottom left of the figure shows the convergence plot of the PSO algorithm. This is a plot showing the cost of moving the particles againt the epochs (or iterations) of the algorithm. It is observed that the line is already flat at 10 epochs. This is the point when a global minima was established by a particle. The iteration did not stop until all other particles converged at that point. At 21 epochs all particls converged at the point and the iteration stopped.
The bottom right reveal verbose statements of the PSO algorithm at the command window of MATLAB. The statement shows that the tuned PID values are:

P = 28, I = 14 and D = 40 at a cost = 422.167

In figure 16 the system is no longer runing at base case. The system is now runing with tuned PID parameters from the PSO algorithm. The result presented, when a load disturbance is applied at area one only, show two graphs (blue and black) that represents frequency responses from the two areas. The black graph represent the response of the thermal plant. This is normal as a disturbance in one area will trigger frequency response, that are different, in both areas. The blue graph represents the response of the system at area two (hydro plant). Again it is observed that this response is still slower than the response in area one.

In figure 17 the system is still runing with tuned PID parameters from the PSO algorithm. The result presented, when a load disturbance is applied at area two only show two graphs (blue and black) that represents frequency responses from the two areas. The black graph represent the response of the thermal plant. This is normal as a disturbance in one area will trigger frequency response, that are different, in both areas. The blue graph represents the response of the system at area two (hydro plant). Again it is observed that this response is still slower than the response in area one.

It is observed that results presented after tuning all brought back the frequency of the load to 50 Hz

Table 1 present the comparison results for figure 4.10 b) using metrics like overshoot, undershoot, settling time and steady state error.

Table 1 result comparison

Algorithm	Overshoot	Undershoot	Settling time	Steady state error
Area 1				
PSO	0.0007	0.0076	55	0
Base line	0	0.0099	55	0.005
Area 2				
PSO	0.012	0.010	55	0
Base line	0.004	0.017	55	0.005

Table 1 uses several metrics to compare the three algorithms tested in this research. It is seen that all two algorithms arrived at the same settling time. The base line algorithm however ended, after 100 seconds, with a steady state error of 0.005 while other algorithms ended with a zero steady state error.

The PSO shows the lowest undershoot performance (0.0076) in area one. All other parameters appera the same because of the synchronizing effet of the hydro-thermal plant.

The PSO gives the best performance.

Figure 18 reveals the graph of the load disturbance and how it affects the turbain speed and the frequency of the power systems in both areas.

Conclusion

This research work modelled a hydro-thermal power plant. The thermal plant section consist of two units each 500 MW of thermal plant while the hydro section consist of a single unit of 500 MW hydro plant. After modelling each section differently, the sections were then hybridized to arrive at the final model. In this research work, it is intended to control the frequency of the system whenever there is a load disturbance. The load disturbance is in the form of sudden change in load (one unit of power) in any or all of the areas. The frequency control is achieved by proper modelling of the governor of the turbines in each component of the hybridized system. Also, for better performance, frequency control is achieved by desiging a secondary controller, which is essentially a PID controller. The controller tuning is achieved using swarm intelligence technique. The PSO algorithm is developed and used to tune the PID controller. Results from base line system performance (PID tuned manually using Ziegler-Nichols method), PSO compared and the results were presented. The following strong points presented can be used to draw conclusions from the results of this research work.

i. At base line performance frequency control was achieved during load disturbance but with frequency deviation of 0.005
ii. At PSO performance frequency control was achieved perfectly with zero frequency deviation during load disturbance after 55 seconds.

PSO gave the best performance.

Recommendation

One of the difficulties encountered during this work is during the tuning of the PID parameters using PSO algorithm. The population of the particles for the search space chosen was with a lot of trial and error. This is because if the wrong particle population is chosing, the particles might get stuck in a local minima. Other machine learning techniques, apart from swarm intelligence technique, like fuzzy logic, Adaptive Neuro-Fuzzy Inference System (ANFIS) can be employed in tuning the PID parameter of the PID controller.

Acknowledgement

This research work wish to acknowlege Tetfund for sponsorship of this research work.

Reference

Akbar, M. I., Kazim, S. A. A., Alrumayh, O., & Khan, Z. A. (2022). A Novel Hybrid Optimization-Based Algorithm for the Single and Multi-Objective Achievement with Optimal DG Allocations in Distribution Networks. *IEEE Access*, *10*. https://doi.org/10.1109/ACCESS.2022.3155484

Ali, E. S., Elazim, S. M. A., Hakmi, S., & Mossad, M. I. (2023). Optimal Allocation and Size of Renewable Energy Sources as Distributed Generations Using Shark Optimization Algorithm in Radial Distribution Systems. *Journal of Energies*, *16*(10), 3983. https://doi.org/10.3390/en16103983

Atkinson, J., & Albayati, I. M. (2021). Impact of the Generation System Parameters on the Frequency Response of the Power System: A UK Grid Case Study. *Journal of Electricity*, *2*, 143-157. https://doi.org/10.3390/electricity2020009

Basu, S. (2018). Modelling of Steam Turbine Generators from Heat Balance Diagram and Determination of Frequency Response. *Control Science and Engineering*, *2*(1), 1-15. https://doi.org/10.11648/j.cse.20180201.11

Elsisi, M., Soliman, M., Aboelela, M. A. S., & Mansour, W. (2024). Bat inspired algorithm based optimal design of model predictive load frequency control. *Electrical Power & Energy Systems*, *83*, 426-433.

Fathy, A., & Kassem, A. M. (2025). Antlion optimizer-ANFIS load frequency control for multi-interconnected plants comprising photovoltaic and wind turbine. *ISA Transactions*, *87*, 282-296.

Guha, D., Roy, P. K., & Banerjee, S. (2023). Load frequency control of interconnected power system using grey wolf optimization. *Swarm and Evolutionary Computation*, *27*, 97-115.

ISSN: 2971-7760 | VOL 6, ISS 3 | 03 AUGUST 2026
https://doi.org/10.5281/zenodo.21778536
NASARAWA STATE UNIVERSITY, KEFFI, NIGERIA

Jagatheesan, Anand, B., Samanta, S., Dey, N., Santhi, V., Ashour, A. S., & Balas, V. E. (2024). Application of flower pollination algorithm in load frequency control of multi-area interconnected power system with nonlinearity. *Neural Computing and Applications*, *28*(1), 475-488.

Lokkas, P., Alamanis, N., Xafoulis, N., & Papageorgiou, G. (2022). An approach on the renewable energy sources. *Operations research*, *3*(2). https://doi.org/10.1007/s43069-022-00138-8

Naghizadeh, R. A., Jazebi, S., & Vahidi, B. (2022). Modeling Hydro Power Plants and Tuning Hydro Governors as an Educational Guideline. *International Review on Modelling and Simulations*, *5*(4), 1780-1790.

Nikhil, P., Ashu, V., & Bhatti, T. S. (2016). Automatic Generation Control of Thermal Power System under Varying Steam Turbine Dynamic Model Parameters Based on Generation Schedules of the Plants. *Journal of Engineering*, *2016*(8), 302-314. https://doi.org/10.1049/joe.2016.0178

Sahu, P. C., Mishra, S., Prusty, R. C., & Panda, S. (2022). Improved-salp swarm optimized type-II fuzzy controller in load frequency control of multi area islanded AC microgrid. *Sustainable Energy, Grids and Networks*, *16*, 380-392.

Wang, Z., Liu, M., Zhao, Y., Wang, C., Chong, D., & Yan, J. (2020). Flexibility and efficiency enhancement for double-reheat coal-fired power plants by control optimization considering boiler heat storage. *Energy 201*, *24*.